Design of Solar Powered Unmanned Biplanes for HALE Missions

Vittorio Cipolla and Aldo Frediani

Nomenclature

AM	Air Mass
AC_V	Aerodynamic centre of vertical surfaces
b	Wingspan
B	Balancing Mass Fraction
CG	Centre of gravity
CP	Centre of pressure
C_L	Lift coefficient
C_D	Drag coefficient
E	Energy
E_A	Aerodynamic efficiency
G_h	Non-dimensional horizontal distance between wings
G_v	Non-dimensional vertical distance between wings
H	Altitude
H_{cruise}	Cruise altitude
m	Pitch moment
mac	Mean aerodynamic chord
M	Mass
MoS	Margin of longitudinal stability
n_z	Vertical load factor
NP	Neutral point
N_V	Number of vertical wings
N_{wt}	Number of wing trunks on half wingspan
P	Power
$P_{\min}$	Minimum required power

V. Cipolla (✉) · A. Frediani
Department of Aerospace Engineering, University of Pisa, Via G. Caruso 8, 56122 Pisa, Italy
e-mail: vittorio.cipolla@for.unipi.it

A. Frediani
e-mail: a.frediani@ing.unipi.it

G. Buttazzo, A. Frediani (eds.), *Variational Analysis and Aerospace Engineering: Mathematical Challenges for Aerospace Design*, Springer Optimization and Its Applications 66,
DOI 10.1007/978-1-4614-2435-2_7,

P_{req}	Required power for cruise flight
Re	Reynolds number
S_H	Horizontal wing area
S_R	Ratio between rear wing and front wing areas
S_V	Vertical wing area
T	Mission endurance
V	Speed
V_{cruise}	Cruise speed
$V_{P_{\text{min}}}$	Minimum required power speed
V_V	Vertical tail volume

Greek Symbols

α	Angle of attack
β	Angle of sideslip
γ	Angle of climb
ΔT_{th}	Endurance variation threshold
ΔM_{th}	Mass variation threshold
ε_g	Energy Density
Φ	Latitude angle
η	Efficiency
ρ	Density

Subscripts

ac	Accumulator
st	Structure
lg	Landing gear
m	Motor
pay	Payload
ch	Charge (ref. to accumulators)
dis	Discharge (ref. to accumulators)
sa	Solar array
sc	Solar cell
p	Propeller
f	Flight
d	Devices
in	Input or initial
out	Output
th	Threshold

Acronyms

AFOV	Angular Field of View
DARPA	Defense Advanced Research Projects Agency
DIA	Department of Aerospace Engineering
ERAST	Environmental Research Aircraft and Sensor Technology
FEM	Finite Element Method

HALE	High Altitude Long Endurance
IFOV	Instantaneous Field of View
IRS	Intelligence, Reconnaissance and Surveillance
LE	Leading edge
NASA	National Aeronautics and Space Administration
SPB	Solar Powered Biplane
TE	Trailing edge
TLC	Telecommunication
UAV	Unmanned Aerial Vehicle
VLM	Vortex-Lattice Method

1 Introduction

In order to perform High Altitude Long Endurance (HALE) missions and be effective, a solar-powered Unmanned Aerial Vehicle (UAV) has to show the fundamental capability to fly continuously, even at high latitudes angles or during Winter. This means that, for each day of mission, during daylight hours the UAV has to collect enough solar energy to feed the propulsion system and to charge the accumulators to be used for night flight. This requirement can be fulfilled only if aerodynamic efficiency of the aircraft is high, which means lightweight structures and high aspect ratio wings.

On the other side, since the long-endurance requirement, such a system has to be reliable, and the lightweight structure has to succeed in facing all the flight loads, including those due to gusts, and to be stiff enough to guarantee the aircraft controllability and manoeuvrability.

The combination of these two aspects can be critical, as the experience of the NASA's prototype Helios has shown. Helios was developed within the Environmental Research Aircraft and Sensor Technology (ERAST) program, with the goal of proving the feasibility of the "eternal flight". After several successful results, the Helios was involved in a fatal accident due to unexpected gusts that made its structure collapse during the second flight test.

The idea on which the present paper is based is the possibility of adopting a different airframe architecture to solve this critical issue, overcoming the limitation of the cantilever wing, which brings to extremely flexible structures that may have unexpected aeroelastic behaviour when flying off-design conditions, as it happened to Helios.

The proposed architecture is a biplane reinforced by several vertical wings that have both aerodynamic and solar collection tasks. This solution, called Solar Powered Biplane (SPB) and shown in Fig. 1, comes from several years of research on box-wing airplanes carried out at Department of Aerospace Engineering (DIA) of Pisa University and, in particular, from a preliminary study in which the potentialities of this solution have been investigated for the first time [11].

Fig. 1 SPB concept

Since the introduction of a new architecture brings new questions about possible reduction in aerodynamic efficiency, increase of the total weight, solar energy collection and flight mechanics behaviour, it is required to verify the aircraft capability of fulfilling the operating requirements with an assigned level of performance. Therefore, this paper aims at:

- proposing an innovative airframe concept that may reduce the risk related to high flexibility of structures;
- defining the SPB sizing process;
- proving the capability of this kind of aircraft of fulfilling the "eternal flight" requirements, defined, according to Defense Advanced Research Projects Agency (DARPA) Vulture Program [5], as follows:
  - latitude up to 45°;
  - 18 000 m as minimum loiter altitude;
  - operative in each year's day.

2 The Solar Powered Biplane Layout

In the present paper, the SPB configuration is introduced under some assumptions [4], according to which the general layout can be simplified as shown in Fig. 2. In such a case, an SPB can be described through the following set of parameters:

- horizontal wing area (S_H);
- wingspan (b);
- number of vertical wings (N_V);
- non-dimensional vertical distance between wings (G_v), defined as the distance, along Z axis, between front and rear wing sections belonging to symmetry plane,

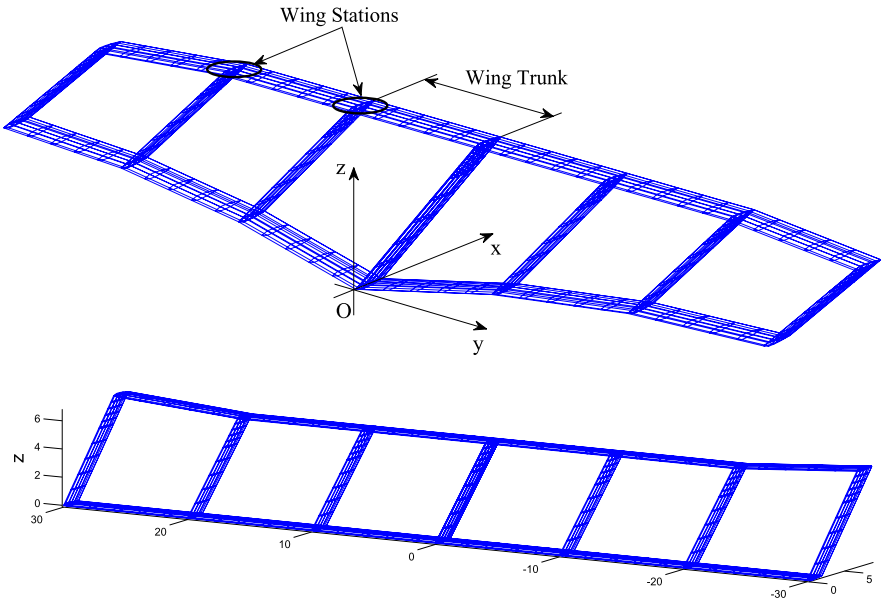

Fig. 2 General (*top*) and simplified (*bottom*) layout of the SPB configuration

divided by b:

$$G_v = \frac{\{Z_{\mathrm{LE2}} - Z_{\mathrm{LE1}}\}_{y=0}}{b}, \tag{1}$$

where LE1 and LE2 indicate the leading edges of wing sections;

- non-dimensional horizontal distance between wings (G_h), taken along X axis and defined as follows:

$$G_h = \frac{\{X_{\mathrm{LE2}} - X_{\mathrm{LE1}}\}_{y=0}}{b}; \tag{2}$$

- ratio between rear wing and front wing areas (S_R).

3 Mission Requirements

Two reference mission types have been selected as the most significant:

- a Telecommunication (TLC) mission, in which the payload is made of antennas;
- an Intelligence, Reconnaissance and Surveillance (IRS) mission, in which electro-optical sensors are mounted on board for image acquisition and remote sensing applications.

It is assumed that each mission has to be performed flying along a closed path that can be considered as elliptical. The dimensions of ellipse axes depend on the foot-

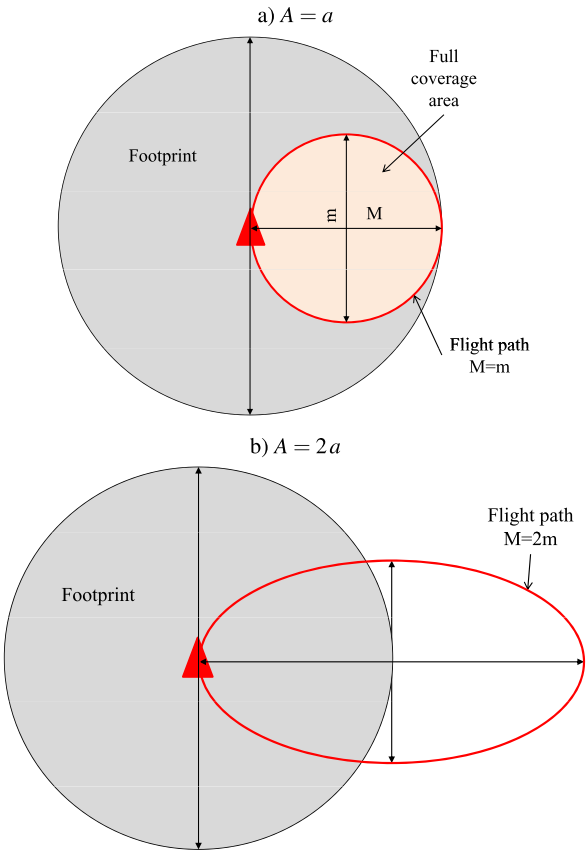

Fig. 3 Effect of flight path on full coverage area dimension

print of payload devices (sensors or antennas) and on the extension of the area that must be served.

Under the assumption

$$a = \frac{\phi_f}{2}, \tag{3}$$

where a is the minor axis length, and ϕ_f is the footprint diameter, the area which can be observed by sensors or antennas from every point of the flight path (*full coverage area*), has maximum extension when major axis (A) is equal to a, i.e. for a circular path (Fig. 3(a)). Increasing A, the covered area will be smaller (b) and disappear when $A = 2a$ (b).

Introducing the ratio between major and minor axes,

$$A_r = \frac{A}{a}, \tag{4}$$

the existence of a full coverage area gives a first constraint on the flight path:

$$A_r < 2. \tag{5}$$

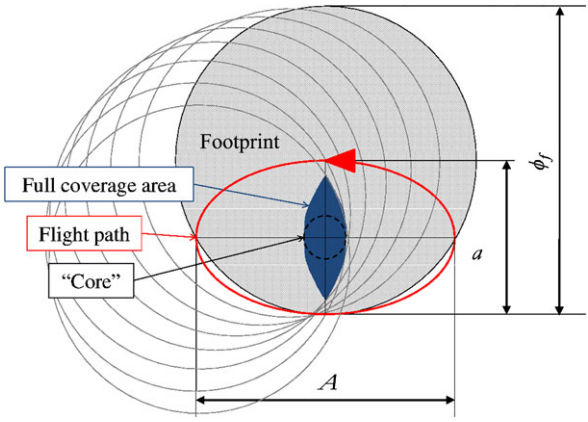

Fig. 4 Flight path, footprint, full coverage area and "core"

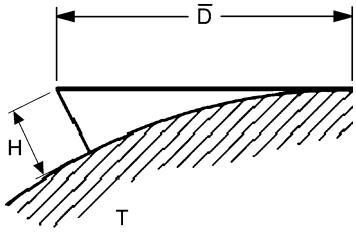

Fig. 5 Radio horizon concept

A conservative estimate of the full coverage area dimension is given by the diameter of the largest inscribed circle, ϕ_c. As shown in Fig. 4, such a circular area is called "core", and ϕ_c is calculated as follows:

$$\phi_c = \phi_f - A. \tag{6}$$

Given Eq. (3) and the definition of A_r, Eq. (6) becomes

$$\phi_c = \left(1 - \frac{A_r}{2}\right)\phi_f. \tag{7}$$

In the next sections, ϕ_c requirements are specialized for TLC and IRS design missions.

3.1 TLC Design Mission

In telecommunications, the operating range of an antenna is given by the *radio horizon*, which is the locus of points at which the direct waves transmitted are tangential to the surface of the Earth.

Hence, for a given antenna located at a height H from Earth, the distance from the radio horizon ($\bar{D}$), also called "line-of-sight", is given by the length of the line

shown in Fig. 5, multiplied by a factor (K), that takes the effect of atmospheric bending on waves into account. Assuming that the Earth is smooth out to the horizon, the communication range can be approximated through the following formula:

$$\bar{D} \simeq K \cdot \sqrt{2RH}, \tag{8}$$

where R is the Earth's radius, whose mean value is 6371 km. As can be found in the literature [1], K is usually taken equal to $\sqrt{4/3}$, which brings to the following formula:

$$\bar{D} \simeq 4124 \cdot \sqrt{H}, \tag{9}$$

with $\bar{D}$ and H in meters.

Approximating the footprint radius with the length $\bar{D}$, it follows that

$$\phi_f = 2 \cdot \bar{D} = 8248 \cdot \sqrt{H}. \tag{10}$$

Hence, substituting Eq. (10) into Eq. (7), the core diameter is given by the function

$$\phi_c = 4214 \cdot (2 - A_r) \cdot \sqrt{H}. \tag{11}$$

The TLC design mission is introduced as follows:

- the core diameter of the served area must be greater than 300 km;
- the flight altitude must be above 14 000 m;
- the mission must be performed also at Winter solstice for latitudes up to 45° North;

At the minimum altitude, ϕ_c is above 300 km for $A_r = 1.4$; hence, mission conditions can be written as follows:

- $A_r = 1.4$;
- $H \geq 14\,000$ m;
- latitude angle $= +45°$;
- Day $=$ 21 Dec (Winter Solstice).

3.2 IRS Design Mission

The IRS mission depends mainly on the electro-optical sensor, whose characteristics are given by the following parameters:

- the Angular Field of View ($AFOV$) angle that, depending on flight altitude (H), defines the footprint width of the sensor (also called *swath width*, Fig. 6):

$$\phi_f = 2H \cdot \tan \frac{AFOV}{2}; \tag{12}$$

by Eq. (7), ϕ_c becomes

$$\phi_c = H \cdot \tan \frac{AFOV}{2} \cdot (2 - A_r); \tag{13}$$

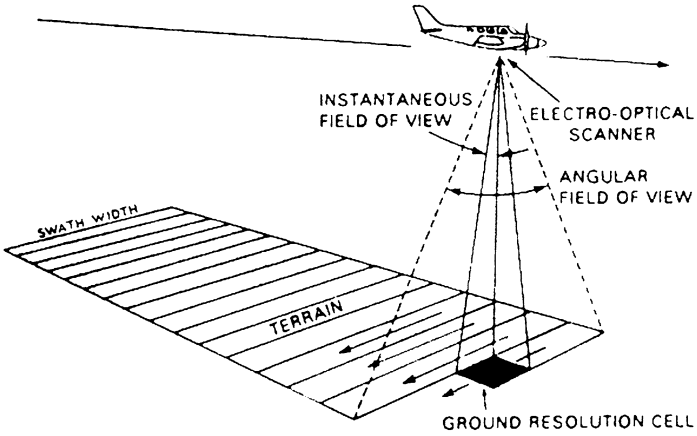

Fig. 6 Instantaneous Field Of View (*IFOV*) and Angular Field Of View (*AFOV*)

- the ground resolution (R_g), defined as the linear dimension of the smallest area on Earth's surface detectable by the sensor. In remote sensing, the ground resolution is commonly described through the Instantaneous Field of View (*IFOV*), which depends on the distance from target (H in this case) and on the number of pixels of the sensor (N_p). The ground resolution can be calculated dividing the swath width by the number of samples (N_p) as follows:

$$R_g = \frac{2H}{N_p} \cdot \tan \frac{AFOV}{2}. \tag{14}$$

When sensor characteristics *AFOV* and N_p are given, the core dimension requirement sets the minimum flight altitude, while the ground resolution one sets the maximum altitude. From (13) and (14) it follows:

$$\frac{\phi_c \cot \frac{AFOV}{2}}{2 - A_r} \leq H \leq \frac{R_g N_p \cot \frac{AFOV}{2}}{2}. \tag{15}$$

Then, the IRS design mission is introduced taking the following requirements into account:

- the surveilled area with core diameter of 2 km;
- the ground resolution of 10 m or less;
- operative also at winter solstice for latitudes up to 45° North.

The given sensor is a hyperspectral camera with the following specifications:

- $AFOV = 18.4°$;
- $N_p = 640$.

Using Eq. (15), altitude constraints are found:

$$\frac{12348}{2 - A_r} \leq H \leq 19757, \tag{16}$$

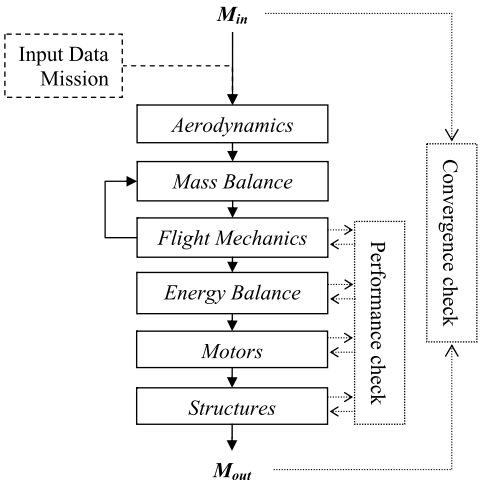

Fig. 7 Overview of the sizing process

where the values are in metres. In order to avoid the air traffic, $H_{\min} = 16000$ is chosen and, therefore, A_r is found from Eq. (16):

$$A_r = 1.22.$$

Therefore, mission conditions are:

- $A_r = 1.22$;
- 15831 m $\leq H \leq$ 19757 m;
- latitude angle $= +45°$;
- Day = 21 Dec (Winter Solstice).

3.3 Payload Requirements

Payload requirements are related to UAV capabilities to fly sensors/antennas with given weight and required power. Such requirements are defined on the basis of previous UAV projects as follows:

- $M_{\text{pay}} = 100$ kg;
- $P_{\text{pay}} = 1$ kW.

4 The Sizing Process

4.1 Overview

The sizing process aims at evaluating the actual aircraft mass (M_{out}) through the steps illustrated in Fig. 7, which are:

- the input mass (M_{in}) definition, where a guess value of the aircraft mass is calculated;
- the aerodynamic analysis, where the minimum required power conditions are calculated;
- the flight mechanics/mass balance cycle, where the equilibrium and stability requirements are met by means of a mass balance strategy;
- the energy balance, where the flight endurance and accumulators mass are calculated;
- the sizing of motors, where the motors mass is defined in order to fulfill the maximum power request;
- the sizing of structures, where the structural components are sized to operate under an assigned stress level.

As the flow chart shows, the process requires the definition of some input data, such as constants and settings for the several models implemented, and mission parameters as defined in Sect. 3.

In addition, Flight Mechanics, energy balance, motors and structures sections are linked to a "Performance check" block, in which other requirements related to expected performance are introduced:

- *Flight Mechanics*
  - trimmed flight;
  - longitudinal stability;
  - directional stability;
  - dihedral effect;
  - spiral stability.
- *Energy Balance*
  - minimum mission endurance (T) given by

$$T_{\min} \geq 24 - \Delta T_{\text{th}} \quad \text{(in hours)}, \tag{17}$$

    where the endurance variation threshold (ΔT_{th}) is set to 0.5 hours, that is, the 2% of the nominal 24 hours mission duration.
- *Structures*
  - maximum structural stress.

If such requirements are met, the sizing process leads to the evaluation of the actual aircraft mass, which is compared to the M_{in} value, in order to check the convergence of the whole process. The convergence requirement is fulfilled if the following inequality holds:

$$|M_{\text{out}} - M_{\text{in}}| \leq \Delta M_{\text{th}}, \tag{18}$$

where mass variation threshold (ΔM_{th}) is the accumulators mass that, for a given configuration and a given required power, if added or removed, gives a flight endurance variation equal to ΔT_{th}. Such definition can also be written as follows:

$$\Delta M_{\text{th}} = \frac{P_{\text{req}} \Delta T_{\text{th}}}{\varepsilon_g}, \tag{19}$$

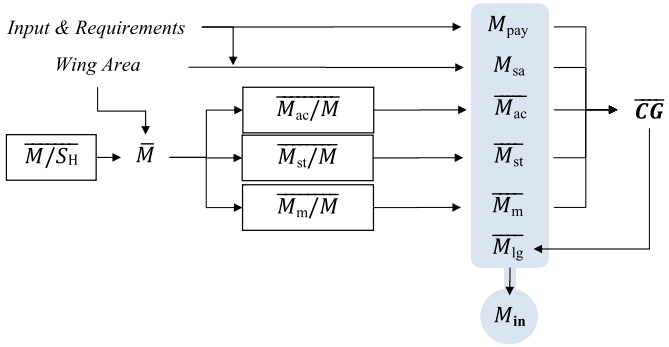

Fig. 8 Flow chart of the input mass evaluation

Table 1 Guess values for input mass evaluation

Guess values	
$\overline{M_{ac}/M}$	50%
$\overline{M_{st}/M}$	25%
$\overline{M_m/M}$	10%
$\overline{M/S_H}$	8–11 kg/m^2

where ε_g is the energy density of the accumulators.

4.2 Input Mass Evaluation

As Fig. 8 shows, the input mass is calculated as follows:

$$M_{in} = M_{pay} + M_{sa} + \overline{M_{ac}} + \overline{M_{st}} + \overline{M_m} + \overline{M_{lg}}, \tag{20}$$

where:

- M_{pay} is the payload mass, given as a requirement;
- M_{sa} is the mass of solar arrays, which can be calculated multiplying the surface density of solar panels by horizontal and vertical wing areas;
- $\overline{M_{ac}}$, $\overline{M_{st}}$ and $\overline{M_m}$ are the guess values of accumulators, structures and motors mass, respectively, which are calculated as fractions of the aircraft guess mass $\overline{M}$. This latter is calculated multiplying the horizontal wing area (S_H) by a guess wing loading value;
- $\overline{M_{lg}}$ is the guess landing gears mass, which depends on the estimated position of the aircraft centre of gravity (CG).

Table 1 shows the typical guess values used in this part of the sizing process.

4.3 Aerodynamics

The aerodynamic analysis aims at finding the minimum value of the required power for cruise flight (P_{req}) and the associated speed ($V_{P_{\min}}$), under the trim constraints. Therefore, the problem to be solved is the following:

$$\begin{cases} \min P_{\text{req}}(V_{\text{cruise}}), \\ C_L = \frac{M_{\text{in}} g}{\frac{1}{2}\rho S_H V_{\text{cruise}}^2}, \\ m|_{CG}(V_{\text{cruise}}) = 0, \end{cases} \tag{21}$$

where V_{cruise} is the cruise speed, C_L is the lift coefficient, g is the acceleration of gravity, ρ is the air density, and m is the pitching moment.

P_{req} is calculated as follows:

$$P_{\text{req}} = \frac{1}{2}\rho S_H V_{\text{cruise}}^3 C_D, \tag{22}$$

where the drag coefficient (C_D) is obtained by summing the following contributions:

- induced drag ($C_{D_{\text{ind}}}$), evaluated by means of a Vortex-Lattice Method (VLM) code, which gives good results in absence of non-lifting bodies;
- airfoil drag ($C_{D_{\text{airf}}}$), including both pressure and friction drag, calculated applying the strip theory to airfoil polar curves;
- friction drag of landing gear fairings, calculated through the flat plate analogy as in [10].

Concerning airfoil drag, it has been observed that a subsonic flow at low Reynolds number (*Re*), as it is for HALE UAVs, pressure drag and friction drag have comparable values and approximated methods which take only friction into account (e.g. flat plate analogy) are not accurate [2]. For this reason, the aforementioned airfoil polar curves have been calculated for different *Re* by means of the code XFOIL and then implemented in the VLM.

Since the parabolic polar curve approximation does not fit the real polar curve trend (Fig. 9) and introduces errors of $\pm 10\%$ on $V_{P_{\min}}$ evaluation, the minimum required power is calculated using an optimization algorithm that finds the local minimum of the continuous single-variable function $P_{\text{req}}(V_{\text{cruise}})$ on a fixed speed interval, typically inside the range 25–40 m/s.

4.4 Flight Mechanics and Mass Balance

Once the minimum power conditions are found, the aircraft mass balance is found by means of an iterative procedure, in order to fulfill the Flight Mechanics requirements, which are:

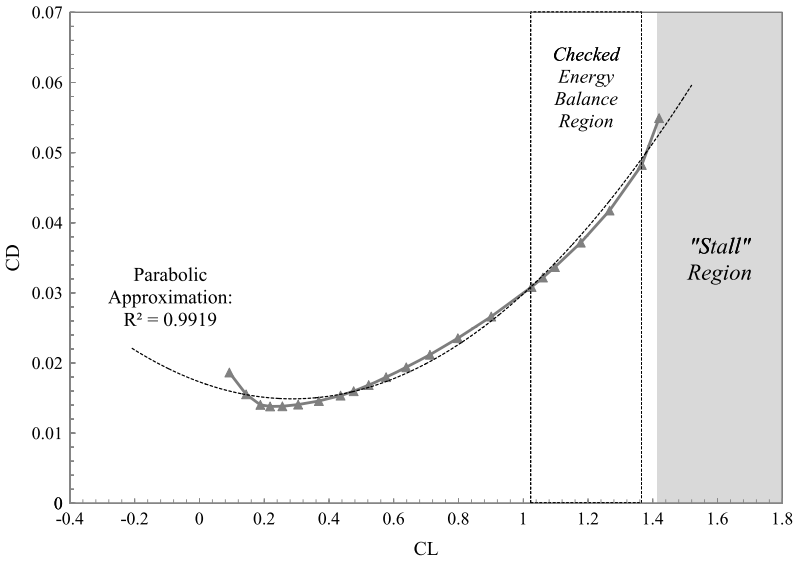

Fig. 9 Example of polar curve and parabolic approximation

- The trim requirement, defined like in Eq. (21), with the pitching moment equilibrium imposed as follows:

$$CP \equiv CG, \tag{23}$$

where CP is the centre of pressure.

- Longitudinal stability requirement, which is given applying upper and lower boundaries to the margin of longitudinal stability (MoS), defined as follows:

$$MoS = \frac{x_{NP} - x_{CP}}{mac}, \tag{24}$$

where x_{NP} and x_{CP} are the longitudinal coordinates of neutral point and centre of pressure, respectively, and mac is the mean aerodynamic chord.

- Directional stability requirement, which is defined by setting a minimum value for the vertical tail volume (V_V), defined as

$$V_V = \frac{S_V(x_{AC_V} - x_{CG})}{bS_H}, \tag{25}$$

where S_V is the vertical wing area, and AC_V is the aerodynamic centre of vertical surfaces.

- Dihedral effect requirement, fulfilled when the following inequality holds:

$$C_{l\beta} < 0, \tag{26}$$

where $C_{l\beta}$ is the change in rolling moment coefficient (C_l) due to a sideslip angle (β) variation.

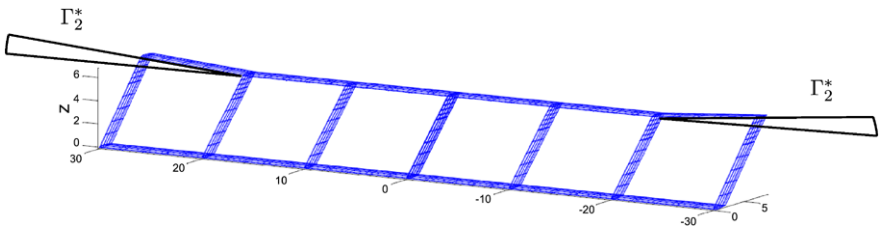

Fig. 10 Rear wing dihedral angles

- Spiral stability requirement, which is expressed as follows:

$$\frac{C_{l\beta}C_{nr}}{C_{lr}C_{n\beta}} > 1, \tag{27}$$

where C_{nr} is the derivative of the yawing moment coefficient (C_n) with respect to yaw rate (r), C_{lr} represents the rolling moment change due to yaw rate, and $C_{n\beta}$ gives the yawing moment variation due to sideslip angle.

Because of the trim constraint, Eq. (24) becomes

$$MoS = \frac{x_{NP} - x_{CG}}{mac}. \tag{28}$$

Therefore, the trim, longitudinal stability and directional stability requirements can be met by changing the distribution of batteries between the two horizontal wings in order to move the aircraft CG.

Dihedral effect and spiral stability requirements, instead, are fulfilled by modifying the dihedral angles of some rear wing trunks (Fig. 10), in order to change the $C_{l\beta}$ value.

4.4.1 Mass Balance Procedure

The mass balance procedure is based on the CG position evaluation, which is performed as follows:

$$\begin{aligned} CG = \frac{1}{M_{\text{in}}}(&M_{\text{pay}}CG_{\text{pay}} + M_{\text{sa}}CG_{\text{sa}} + \overline{M_{\text{ac}}}CG_{\text{ac}} \\ &+ \overline{M_{\text{st}}}CG_{\text{st}} + \overline{M_{\text{m}}}CG_{\text{m}} + \overline{M_{\text{lg}}}CG_{\text{lg}}), \end{aligned} \tag{29}$$

where subscripts have the same meaning as in Eq. (20). Then, the following assumptions are made:

- the payload mass can be positioned in order to have a small influence on the CG location; hence,

$$CG_{\text{pay}} \equiv CG;$$

- the structural components and solar arrays can be assumed as homogeneously distributed on both wings; therefore,

$$CG_{\mathrm{st}} \equiv CG_{\mathrm{sa}}.$$

Given these assumptions, Eq. (29) becomes

$$\begin{aligned} CG = \frac{1}{M_{\mathrm{in}} - M_{\mathrm{pay}}} \big[&(\overline{M_{\mathrm{st}}} + M_{\mathrm{sa}}) CG_w \\ &+ \overline{M_{\mathrm{ac}}} CG_{\mathrm{ac}} + \overline{M_{\mathrm{m}}} CG_{\mathrm{m}} + \overline{M_{\mathrm{lg}}} CG_{\mathrm{lg}} \big], \end{aligned} \tag{30}$$

where CG_w indicates the centre of gravity of horizontal and vertical wings, which coincides with CG_{st} and CG_{sa}.

The first step of the mass balance procedure consists in assuming that the centres of gravity of accumulators and horizontal wings (CG_{wH}) coincide, which means that the accumulators are considered as homogeneously distributed on horizontal wings. Therefore, the starting condition can be described as follows:

$$\begin{cases} M_{\mathrm{ac}_1} + M_{\mathrm{ac}_2} = \overline{M_{\mathrm{ac}}}, \\ \frac{M_{\mathrm{ac}_2}}{M_{\mathrm{ac}_1}} = S_R, \end{cases} \tag{31}$$

where subscripts 1 and 2 indicate front and rear wings, respectively, and S_R is the ratio between rear wing and front wing areas. Hence, batteries repartition on the two wings is given by

$$\begin{cases} M_{\mathrm{ac}_1} = \frac{1}{S_R+1} \overline{M_{\mathrm{ac}}}, \\ M_{\mathrm{ac}_2} = \frac{S_R}{S_R+1} \overline{M_{\mathrm{ac}}}. \end{cases} \tag{32}$$

The balancing process aims at finding the amount of batteries M^*_{ac} that has to be moved from the rear wing to the front one, in order to meet the Flight Mechanics requirement.

Introducing the Balancing Mass Fraction (B) as

$$B = \frac{M^*_{\mathrm{ac}}}{M_{\mathrm{ac}_2}}, \tag{33}$$

the modified battery repartition becomes

$$\begin{cases} M'_{\mathrm{ac}_1} = (1 + B \cdot S_R) \frac{1}{S_R+1} \overline{M_{\mathrm{ac}}}, \\ M'_{\mathrm{ac}_2} = (1 - B) \frac{S_R}{S_R+1} \overline{M_{\mathrm{ac}}}. \end{cases} \tag{34}$$

B is used to control the balancing procedure convergence: when $B > 1$, a divergence occurs, and Flight Mechanics requirements cannot be fulfilled. It has been observed that feasible solutions have $B < 0.5$.

Given the definition of B, the mass balance procedure is described here below:

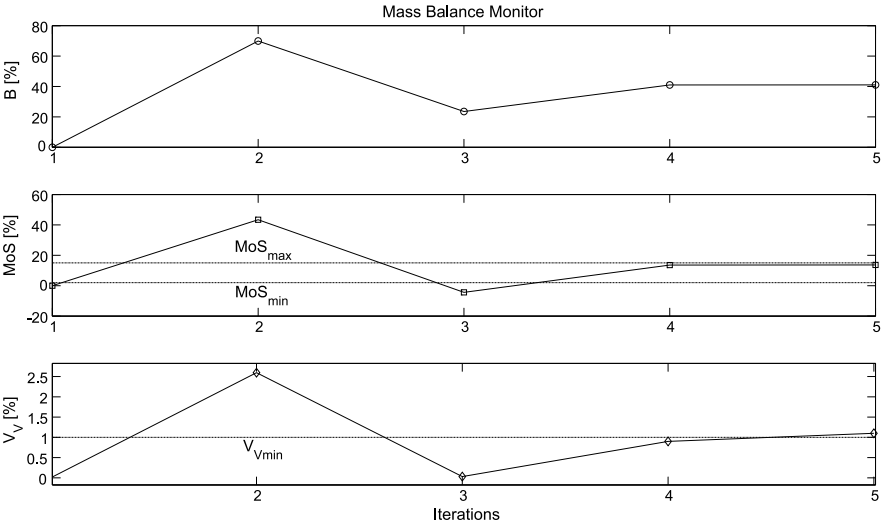

Fig. 11 Mass balance process

1. the results from Aerodynamics section provide initial flight mechanics characteristics, such as the neutral point (*NP*) and the aerodynamic centre of vertical surfaces (AC_V);
2. the *CG* longitudinal position is imposed as follows:

$$x_{CG} = \min\left(x_{NP} - MoS_{\min} \cdot mac, x_{AC_V} - V_{V_{\min}} \cdot \frac{S_H}{S_V} \cdot b\right); \tag{35}$$

3. the associated value of B is calculated;
4. if $B < 1$, the procedure continues, and trim conditions on lift and pitch moment are imposed;
5. the aerodynamic and flight mechanic characteristics are calculated by means of the VLM code, in which the trim requirement in Eq. (23) is met by modifying the angles of incidence of front and rear wings;
6. new values of *NP* and AC_V are calculated.

The procedure is reiterated from point 2 and stops if both requirements on *MoS* and V_V are fulfilled or if $B > 1$. In the first case, Flight Mechanics check is passed, otherwise the sizing process is stopped. Figure 11 shows an example of the balancing process iterations.

4.5 Energy Balance Evaluation

According to the scheme in Fig. 12, the main variables involved in energy balance evaluation are the following:

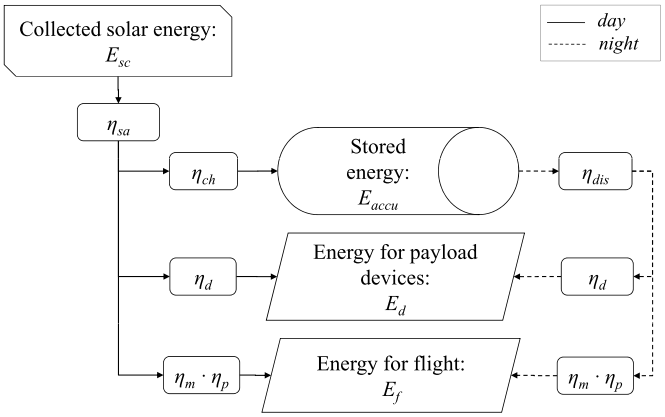

Fig. 12 Flow chart of the daily energy balance

- η_{sa}: solar array efficiency calculated taking Albedo effect into account;
- η_{m}: brushless motors efficiency;
- η_{p}: propeller efficiency;
- η_{d}: efficiency of payload devices (electro-optical sensors or antennas);
- η_{ch}: accumulators charge efficiency;
- η_{dis}: accumulators discharge efficiency;
- E_{sc}: collected solar energy;
- E_{f}: required energy for flight;
- E_{d}: energy required to feed payload devices;
- E_{ac}: energy stored in the accumulation system.

Energy balance can be "checked" when the energy flowing through accumulators during one day, ΔE_{ac}, is 0, "unchecked" if $\Delta E_{\mathrm{ac}} < 0$ and "over-checked" if $\Delta E_{\mathrm{ac}} > 0$.

If the energy balance is checked or over-checked, the aircraft is able to use solar energy to feed motors and devices during daylight hours and to charge batteries with an amount of energy that is sufficient to fly with all systems working during the night. In the second case, the exceeding energy can be used to feed optional devices, to climb and fly at a higher altitude or for speed variations.

Hence, the starting equation for energy balance evaluation is the following:

$$\Delta E_{\mathrm{ac}} = 0, \tag{36}$$

which can be written as the balance between the energy stored during daylight E_{ac}^{D} and the energy released during night E_{ac}^{N}:

$$E_{\mathrm{ac}}^{D} - E_{\mathrm{ac}}^{N} = 0. \tag{37}$$

The time intervals indicated by superscripts D and N depend on the collected solar power (P_{sc}), the required power for flight (P_{f}) and the required power for devices (P_{d}). They are defined as follows:

- D is the time interval in which solar panels suffice in providing power to motors and payload devices:

$$P_{\text{sc}}\eta_{\text{sa}} \geq \frac{P_{\text{f}}}{\eta_{\text{m}}\eta_{\text{p}}} + \frac{P_{\text{d}}}{\eta_{\text{d}}}; \tag{38}$$

- N is the time interval in which energy provided by solar panels is not sufficient to feed motors and payload devices and accumulators' contribution is required:

$$P_{\text{sc}}\eta_{\text{sa}} < \frac{P_{\text{f}}}{\eta_{\text{m}}\eta_{\text{p}}} + \frac{P_{\text{d}}}{\eta_{\text{d}}}. \tag{39}$$

The energy stored during daylight is obtained as follows:

$$E_{\text{ac}}^{D} = \eta_{\text{ch}}\left(\eta_{\text{sa}}E_{\text{sc}} - \frac{E_{\text{f}}^{D}}{\eta_{\text{m}}\eta_{\text{p}}} - \frac{E_{\text{d}}^{D}}{\eta_{\text{d}}}\right), \tag{40}$$

while the energy spent during night time is given by

$$E_{\text{ac}}^{N} = \frac{1}{\eta_{\text{dis}}}\left(\frac{E_{\text{f}}^{N}}{\eta_{\text{m}}\eta_{\text{p}}} + \frac{E_{\text{d}}^{N}}{\eta_{\text{d}}}\right). \tag{41}$$

Substituting Eq. (40) and Eq. (41) into Eq. (37), the energy balance equation is obtained:

$$\eta_{\text{sa}}E_{\text{sc}} = \left[\frac{E_{\text{f}}^{D}}{\eta_{\text{m}}\eta_{\text{p}}} + \frac{E_{\text{d}}^{D}}{\eta_{\text{d}}} + \frac{1}{\eta_{\text{ac}}}\left(\frac{E_{\text{f}}^{N}}{\eta_{\text{m}}\eta_{\text{p}}} + \frac{E_{\text{d}}^{N}}{\eta_{\text{d}}}\right)\right], \tag{42}$$

where η_{ac} is the accumulator charge/discharge efficiency, given by

$$\eta_{\text{ac}} = \eta_{\text{ch}} \cdot \eta_{\text{dis}}. \tag{43}$$

It is assumed that charge and discharge efficiencies are equal, and therefore,

$$\eta_{\text{ch}} = \eta_{\text{dis}} = \sqrt{\eta_{\text{ac}}}. \tag{44}$$

If the energy balance is checked or over-checked, the accumulators mass is calculated dividing the energy spent for night time flight by the Energy Density (ε_g) of accumulation system:

$$M_{\text{ac}} = \frac{E_{\text{ac}}^{N}}{\varepsilon_g}. \tag{45}$$

4.5.1 Incoming Solar Energy Model

The total incoming radiation (I_{tot}) is calculated through the following formula:

$$I_{\text{tot}} = I \cdot (\tau_b + \tau_d)^{AM}, \tag{46}$$

where

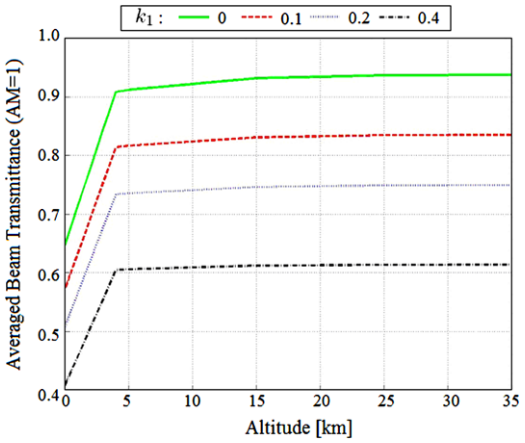

Fig. 13 Averaged beam radiation coefficient [11]

- I is the incoming solar power collected by a panel with unitary area, which depends on the angle of incidence of sunbeams respect to the normal direction to panel surface and is calculated as in [6];
- τ_b is the beam radiation coefficient, given by

$$\tau_b = \tau_{\text{scatt}}(\lambda_w, H, k_1, k_2) \cdot \tau_{\text{abs}}(\lambda_w, H, k_1), \tag{47}$$

where τ_{scatt} is the scattering coefficient due to particles (air, dust and water vapor), τ_{abs} is the absorption coefficient due to ozone and water vapour, λ_w is the radiation wavelength, H is the altitude, k_1 is the turbidity coefficient ($0 =$ clear conditions, $0.4 =$ very turbid conditions), and k_2 is related to aerosols size.

According to previous works [11, 12], air scattering is evaluated with the Reyleigh model, water and dust scattering by means of the Ångström model and the absorption coefficient, assumed constant for altitudes between 3000 and 20 000 m, as a function of the atmospheric turbidity. Because of water vapour presence, λ_w effect is important only at low altitudes, where the aircraft flies for short periods. Therefore, it is possible to approximate τ_b with the λ_w averaged value, which depends on altitude and turbidity coefficient as Fig. 13 shows;

- τ_d is the diffused radiation coefficient, which is much smaller than the direct one and can be neglected [6];
- AM is the Air Mass, which represents the ratio between the actual distance covered by sunbeams to reach the panel and the minimum possible distance. It is related to the zenith angle (θ_z) through the following expression:

$$AM = \frac{1}{\cos\theta_z}. \tag{48}$$

4.5.2 Collected Solar Energy Model

The model used to calculate energy collected by solar panels take the following aspects into account:

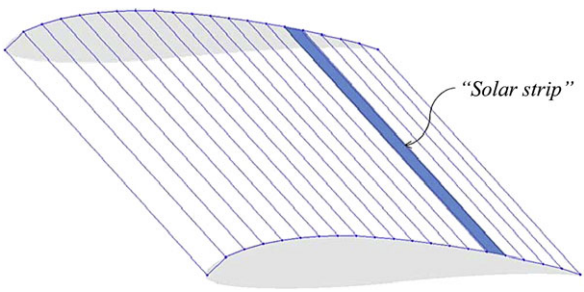

Fig. 14 Strip of solar panels on a wing surface

- solar cells on horizontal wings are placed on the upper surface and preserve the airfoil shape;
- solar cells on vertical wings are placed on both sides and preserve the airfoil shape;
- panels are defined as "strips", whose chordwise dimension is given by cell length and spanwise length is the wing trunk span (Fig. 14);
- angle of attack, angle of trajectory, angle of climbing and angles of incidence (one for each horizontal wings) contribute in panel elevation angles;
- at each time step in which the mission is discretized, the aircraft orientation is calculated in order to find the azimuth angle of panels.

For a given time (t), the total solar power collected by panels on aircraft is calculated as follows:

$$P_{\mathrm{sc}}(t) = \sum_{w} \left[\sum_{i} I_i(t) \cdot S_i \right]_w (\tau_b + \tau_d)^{AM(t)}, \tag{49}$$

where subscript w indicates a generic wing (horizontal or vertical), and subscript i indicates a generic solar panel strip having area S_i. For each strip, the term I_i is calculated taking the panel orientation (elevation and azimuth angles) and the mission condition (latitude, declination and hour angles) into account.

Since panel angles change as the aircraft moves along the flight path, the mission is divided in time steps, and for each of them, P_{sc} is evaluated. For each of these intervals, P_{sc} value is used to verify Eq. (38) or Eq. (39), and, if the first one holds, it is integrated to calculate the energy balance term E_{sc} (see Eq. (42)).

Details on power collection for a typical winter mission are shown in Fig. 15, where the chord station is 0% at the leading edge and 100% at the trailing edge.

4.6 Structures Sizing

The model for structures sizing is based on previous works [3, 9], whose achievements have been the determination of the SPB flight envelope, the definition of a design solution for the main components and the evaluation of the admissible stress level by means of Finite Element Methods (FEMs).

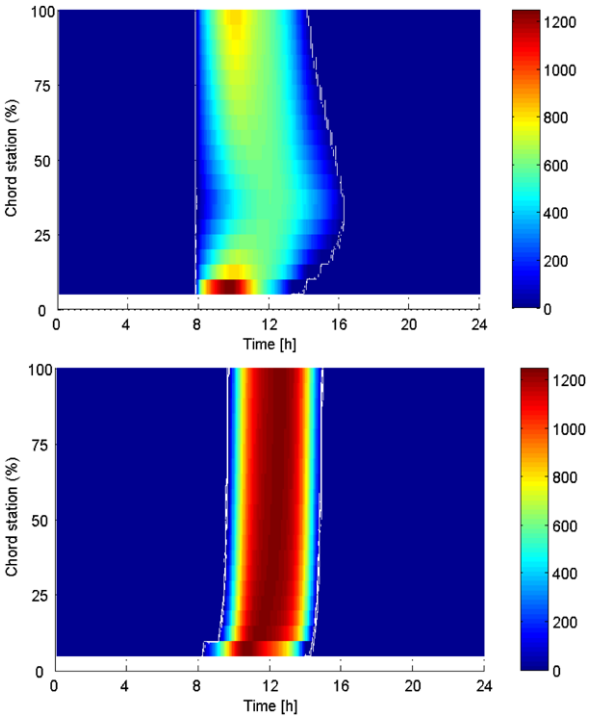

Fig. 15 Solar power per area unit collected by horizontal (*top*) and vertical (*bottom*) wings

4.6.1 The Flight Envelope

The flight envelope has been found according to MIL-F-8785C, MIL-STD-1797A and FAR regulations, adopting the $1 - \cos$ discrete model for gust loads. A reference SPB configuration, designed for Winter missions, has been considered, and it has been found that, because of the low wing load of such a kind of aircraft, the maximum load factors (n_z) are those due to gusts (Fig. 16).

As Fig. 17 shows, the n_z limit values are obtained for altitude around 10 000 m, at which the aircraft flies only for short periods, during climb and descent. Therefore, the related n_z values ($+6.5$ and -4.5) have been indicated as ultimate and then used for structural sizing.

4.6.2 The Design Solution

Concerning the design solution, structure components of each wing trunk, horizontal or vertical, have the same design scheme, which is shown in Fig. 18 and described hereafter:

- each wing section has a double spar, which provides a high bending stiffness;
- in order to improve the torsional stiffness, spars have a closed cross-section;

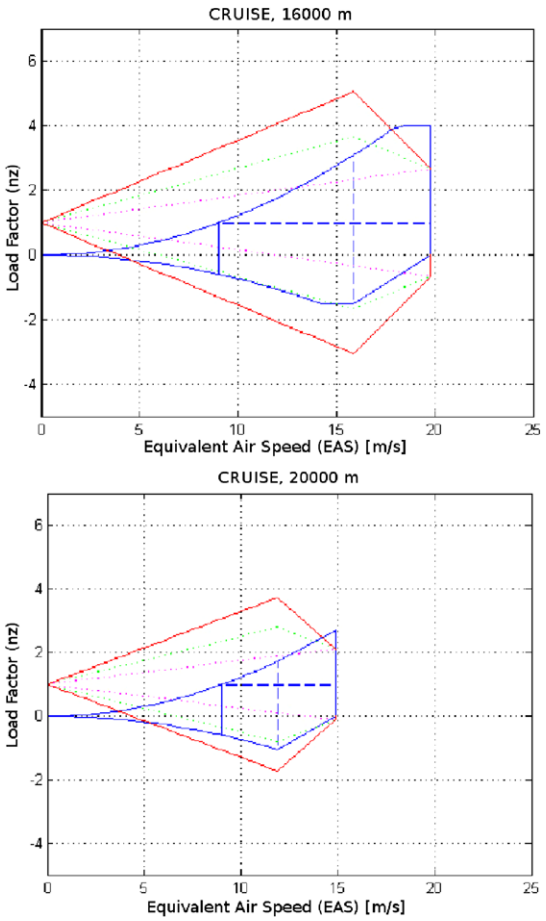

Fig. 16 Flight envelope at 16 000 m (*top*) and 20 000 m (*bottom*) [3]

- ribs consist of trusses placed at constant distance along the wingspan;
- spars and ribs are made of laminates of Carbon-Epoxy plies of thickness above 1 mm.

Spar sections are shaped in order to fit exactly inside wings, in order to provide a physical connection to solar panels with no need of other components. As shown in Fig. 19, the sizing parameters for leading edge (LE) and trailing edge (TE) spars are the width (w_{LE}, w_{TE}) and the average wall thickness (t).

4.6.3 FEM Analyses

By means of a commercial FEM code, static and buckling analyses have been carried out taking maximum (positive and negative) load factors conditions and impact at landing into account. For static analyses, spars and ribs have been modelled

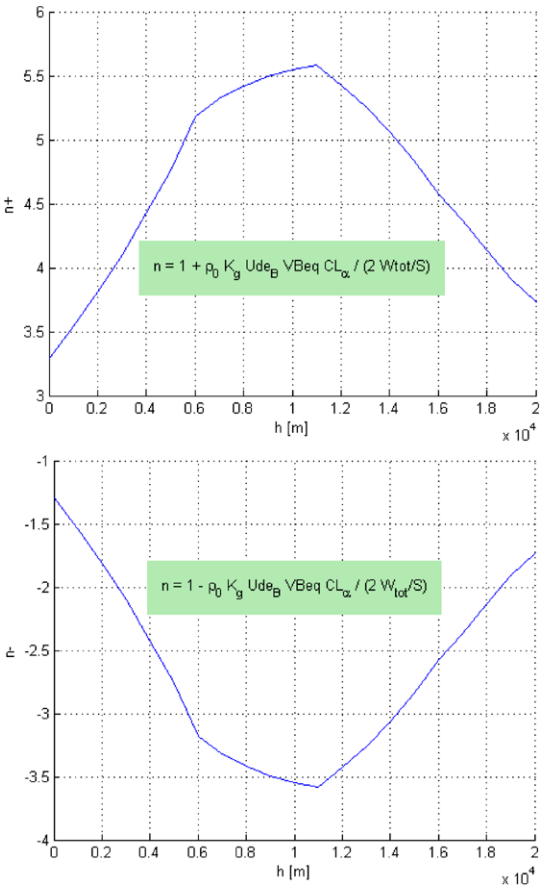

Fig. 17 Maximum positive (*top*) and negative (*bottom*) load factors at various altitudes [3]

by means of beam elements, while shell elements have been used to model spars' walls.

The structural components have been sized on the basis of FEM results, and the following achievements have been reached:

- at every load condition, stresses are below the *first-ply-failure* values of the composite material;
- at every load condition, the twist due to wing deformation does not provoke stall in any section;
- buckling phenomena take place on the internal and lower walls of the spars, where the integrity of cells is not affected (Fig. 20). The "allowed buckling" cases are indicated in Table 2, in which it can be observed that load factors intervals are compatible to the maximum and minimum values calculated from flight envelope.

As a further result, a distribution scheme for battery packs has been defined under the constraint of avoiding the impact of front wing on the ground during landing.

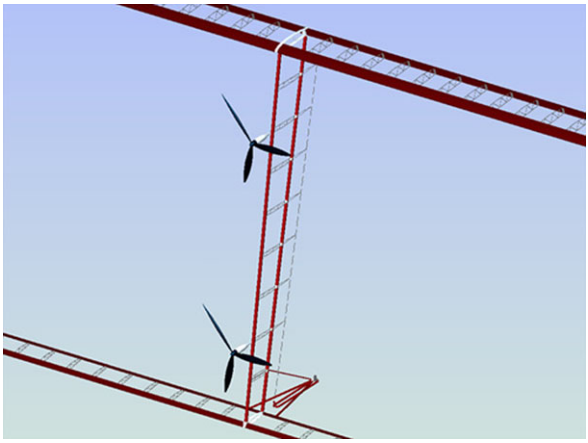

Fig. 18 Overview of the SPB main structures [9]

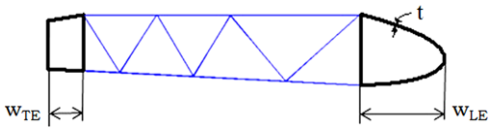

Fig. 19 Sizing parameters for spars

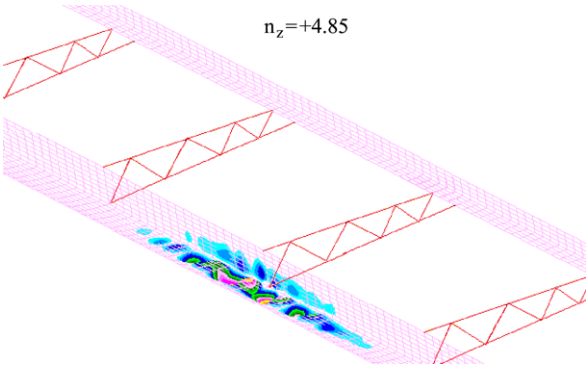

Fig. 20 "Allowed buckling" on a LE beam at positive load factor [9]

Table 2 Load factors intervals for "allowed buckling" on front and rear wing structures

Front wing	
Positive load factors	$+4.6 < n_z < +6.5$
Negative load factors	$-4.5 < n_z < -2.3$
Rear wing	
Positive load factors	$+6.6 < n_z <$ n.c.
Negative load factors	$-4.4 < n_z < -2.2$

4.6.4 Model for Structures Sizing

The structural model has been built on the basis of the assumption, derived from FEM results, that the sizing condition is given by the buckling absence requirement at the maximum positive load factor ($n_z = +6.5$). In addition, it has been observed that rear wing structures experience the highest stress levels, and hence a simplified model can be derived, isolating the rear wings and introducing the internal forces calculated through by FEM simulations. By means of this model, the bending moment distribution and the maximum tensile stress are then calculated.

According to the previous assumption and FEM results, a structural configuration able to fulfill the given requirements is characterized by Von Mises stress levels below 300 MPa at the maximum load factor condition. This characterization has been used to define a sizing criterion for the design of beams: the structure is efficient if the maximum Von Mises stress ($\sigma_{\max}$) is close to the "operating stress" (σ_{oper}) of 300 MPa, as expressed in the following relation:

$$\frac{|\sigma_{\max} - \sigma_{\text{oper}}|}{\sigma_{\text{oper}}} \leq 5\%. \tag{50}$$

The inequality in Eq. (50) represents the performance requirement for structures sizing, which is achieved, when possible, through the following procedure:

1. the initialization consists of setting the sizing parameters w_{LE}, w_{TE} and t to their minimum value;
2. while t is kept constant, $\sigma_{\max}$ is calculated for all the allowed combinations of w_{LE} and w_{TE};
3. if one or more (w_{LE}, w_{TE}) combinations meet the performance requirement, the solution is the one with the lowest structural mass, otherwise t is increased, and the procedure is repeated from previous step;
4. if a combination (t, w_{LE}, w_{TE}) does not exist, the structural sizing cannot be performed, and the SPB configuration is discarded.

4.7 Motors Sizing

The model for brushless motors sizing is taken from [11], in which the following statistical relation is used:

$$M_{\text{m}} = 0.0045 \cdot P, \tag{51}$$

where motor mass (M_{m}) is in kg, and the nominal power (P) is in W.

Observing that the power required for flight is obtained multiplying nominal power by motor efficiency (η_{m}) and propeller efficiency (η_{p}), Eq. (51) becomes

$$M_{\text{m}} = 0.0045 \cdot \frac{P_{\max}}{\eta_{\text{m}}\eta_{\text{p}}}. \tag{52}$$

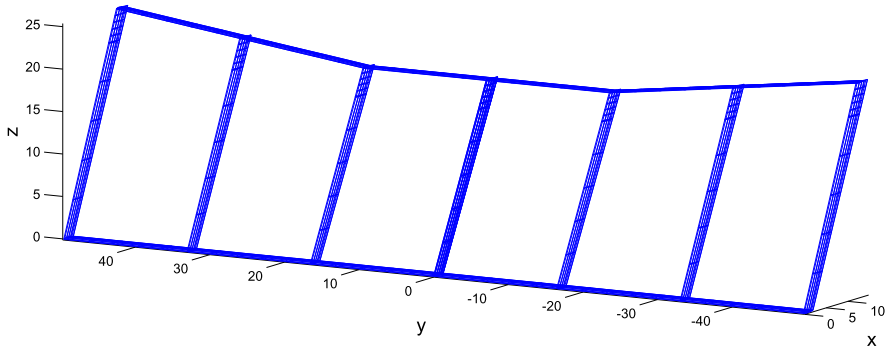

Fig. 21 SPB configuration for Winter TLC missions at 18 000 m

Therefore, the mass of the entire propulsion system can be defined by means of the maximum power request ($P_{\max}$) that the aircraft experiences during the mission. Such a value is found when the aircraft, flying at the maximum required altitude, climbs with a given angle of climb (γ). In such case, the required power has the following expression:

$$P_{\max} = P(H_{\max}) + \sqrt{\frac{(Mg)^3}{\rho(H_{\max}) S_H C_L}} \sin\gamma, \tag{53}$$

where C_L is referred to level flight at $H_{\max}$.

5 Results

In [4] the sizing process here presented has been implemented in an optimization problem, aiming at finding minimum mass SPB configurations, under different mission requirements.

In this paper, one of the most significant result is shown: it is an SPB designed for TLC missions at latitude of 45° and cruise altitude above 18 000 m. It has been found that such a configuration can operate continuously in each year's day and, therefore, is able to meet the aforementioned DARPA requirements.

A scheme of this solution is given in Fig. 21, and its main characteristics are listed in Table 3. It is worth noticing that the predicted Aerodynamic Efficiency is 38, which is comparable to other HALE UAVs (Fig. 22).

As a further result, Fig. 23 shows two *Operating Domains* used to evaluate the flexibility of such aircraft in performing TLC and IRS missions.

The Operating Domain is a design tool, introduced in [4], which consists of a chart, where, for each altitude, the region of the Day-Φ plane in which the given configuration can fulfill the energy balance requirement is represented. Such a region, assumed to be symmetric to acsLat = 0° and Summer Solstice axes, is bounded from above by a parabolic arc, whose vertex belongs to the Winter Solstice axis.

Table 3 Data of the SPB for Winter TLC missions at $H_{\text{cruise}} = 18\,000$ m and $\Phi = 45°$

DESIGN PARAMETERS	
S_H	392.4 m^2
b	99.1 m
G_v	0.214
S_R	0.8
G_h	0.12
N_V	7
CHARACTERISTICS	
M	3525 kg
M/S_H	9 kg/m^2
V_{cruise}	33.5 m/s
P_{req}	30509 W
P_{req}/S_H	78 W/m^2
ΔT	−0.3 h
E_A	38
MoS	19.9%
V_V	1.02%
P_{pay}	1000 W
M_{pay}	100 kg
ϕ_c	340 km

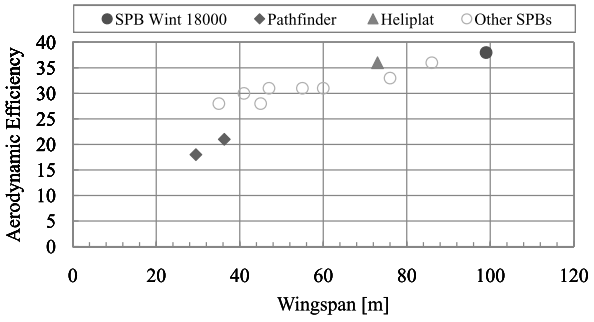

Fig. 22 Comparison between aerodynamic efficiencies

The vertex ordinate is the maximum Φ for which the aircraft is operative, i.e. it can fly continuously, at the given loiter altitude. Since the solar energy model is not valid for latitudes above 70°, in any case the chart is limited by the $\Phi = 70°$ line.

The Operating Domain analysis shows that such aircraft can perform both TLC and IRS missions: altitudes above 20 000 m can be reached at latitudes up to 16° (TLC) and 4° (IRS), while, at the minimum altitude of 16 000 m, the highest operating latitudes are 50° (TLC) and 38° (IRS).

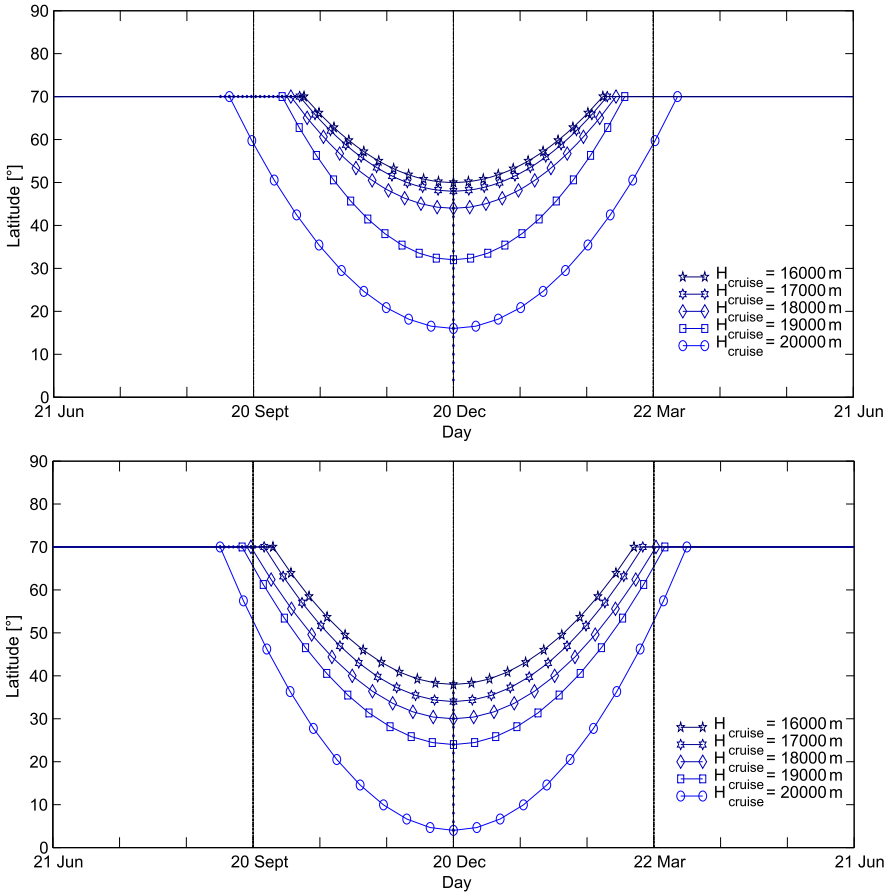

Fig. 23 Operating domain of the 18 000 m, winter SPB for TLC (*top*) and IRS (*bottom*) missions

6 Structural Design Review and Aeroelastic Analysis

The SPB configuration described in Sect. 5 has been the object of aeroelastic analyses inside the M.Sc. Thesis work carried out at DIA [8]. Such analyses have been performed by means of the software MSC Nastran, taking the structure resulting form the aforementioned sizing process as a starting point.

Beside the aeroelastic studies, one of the outcomes of this work has been a design review of wing structures, in which the D-shaped front beam of each wing has been replaced with a multi-box beam obtained by adding an internal vertical wall inside the previous section. This type of structure, Fig. 24, has been verified for static and buckling loads and has been chosen in order to improve the technological feasibility of the solution.

Concerning the static analysis, it has been observed that the in-plane stiffness of vertical wings requires an improvement, since the loading condition associated

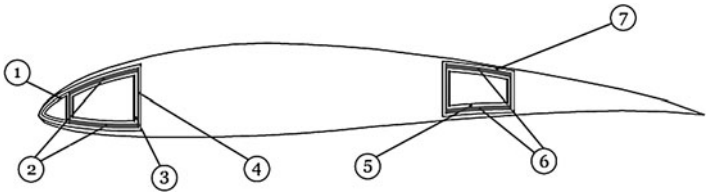

Fig. 24 The modified wing section structures [8]

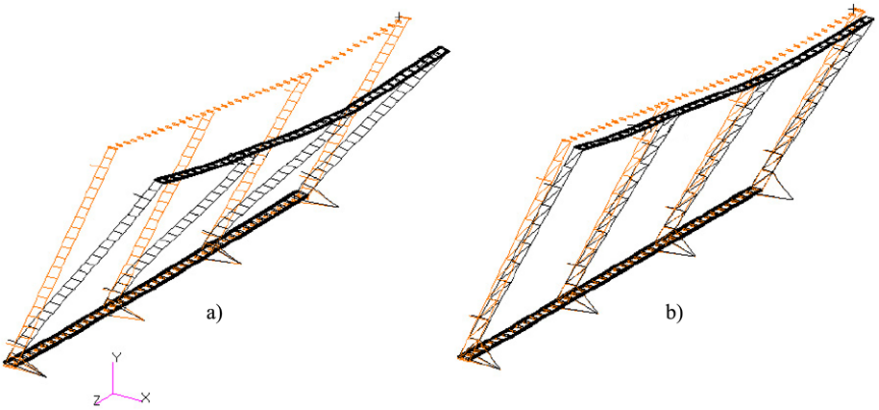

Fig. 25 Stiffness improvement due to internal braces presence (*right*) on vertical wings [8]

to ground manoeuvres, in which the lift force is absent, causes significant deformations. Therefore, the wing design has been modified, increasing the distance between ribs and adding internal braces, which can reduce the rear wing displacement (Fig. 25).

Once static and buckling requirements have been fulfilled, the aeroelasticity of the SPB has been analysed, focusing on both steady and dynamic phenomena.

6.1 Steady Aeroelasticity

From the steady standpoint, it has been observed that the difference in deformations between rigid trim and flexible trim cases depends on the horizontal wings local equilibrium between lift and weight. In particular, when the weight distribution does not equilibrate the lift distribution, as it happens at wing tips, where lift decreases, aeroelastic effects on lift can be great (Fig. 26).

Although it has been found that such effects do not cause divergence, it is better to have them under control, hence a possible solution is to change the accumulators distribution along wingspan in order to achieve the local equilibrium. Figure 27 shows the distribution of batteries which minimizes this effect, and, as said before, it is worth noticing that its characteristic is an unloaded area close to wing tip.

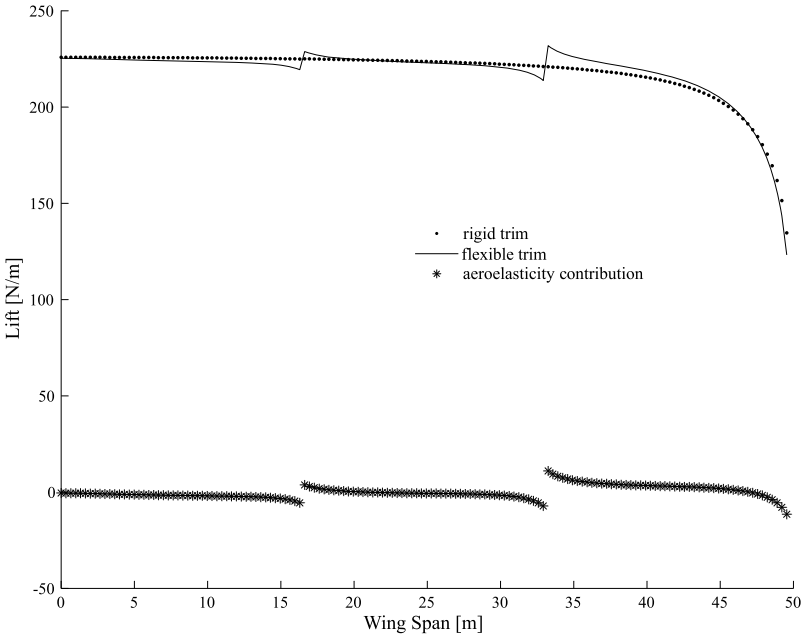

Fig. 26 Initial lift distributions along wingspan for rigid and flexible trim cases on front wing [8]

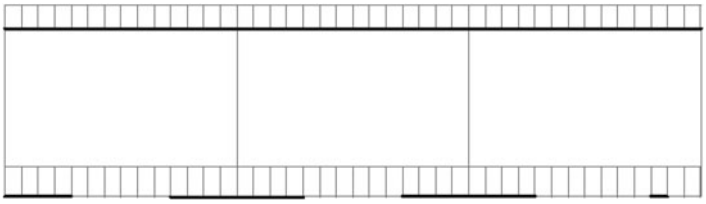

Fig. 27 Final distribution of batteries along wingspan [8]

As a result, in cruise condition the weight distribution given by such accumulator layout gives a maximum displacement of 0.65 m (0.6% of wingspan) against 5.24 m (5.2% of wingspan) obtained considering batteries also on wing tips. As a consequence, this layout minimizes also the steady aeroelasticity effects; Fig. 28, in fact, shows the small difference between rigid and flexible trim cases.

6.2 Dynamic Aeroelasticity

The dynamic aeroelasticity study has been focused on flutter and, as a first case, the SPB configuration modified with internal braces on vertical wings and the afore-

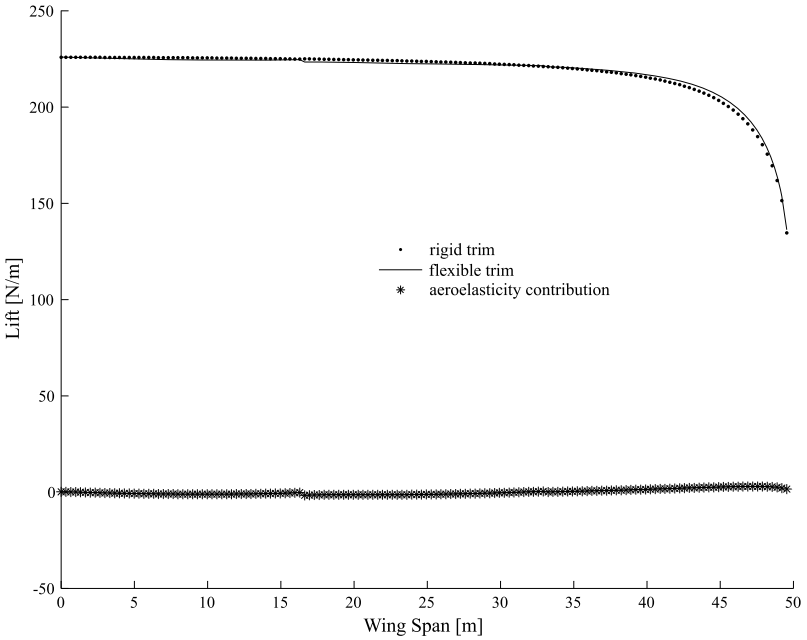

Fig. 28 Final lift distributions along wingspan for rigid and flexible trim cases on front wing [8]

Table 4 Structural modes of the initial configuration

Mode	Frequency [Hz]	Deformation
1	0.06	Bending out of the horizontal plane (mainly)
2	0.08	Bending inside the horizontal plane (mainly)
3	0.11	Torsion around wingspan direction (mainly)
4	0.30	Bending out of the horizontal plane (mainly)
5	0.38	Bending and torsion
6	0.47	Bending and torsion

mentioned batteries distribution, has been analysed by means of the $p - k$ method applied to the cruise condition, for speed between 10 m/s and 80 m/s.

The first six structural modes, for which details are given in Table 4, have been recognized as significant, and the associated flutter analysis has shown that the 2nd mode, which causes a bending almost inside the horizontal plane, is not damped ($g > 0$, Fig. 29).

The cause of such a behaviour has been found in the poor in-plane stiffness of the considered double-spar structure. As already done for vertical wings, the solution found is the addition of internal braces and the reduction of ribs, for both front and rear wings (Fig. 30).

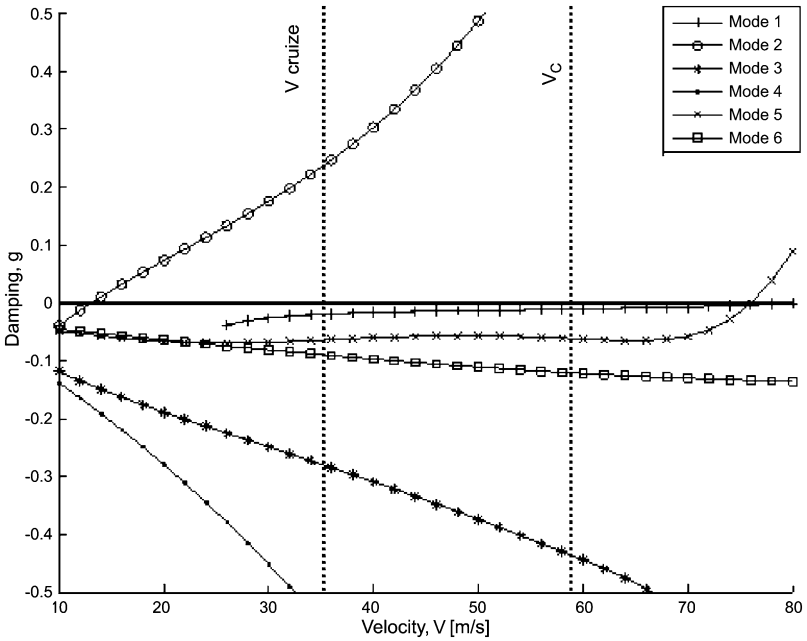

Fig. 29 Flutter diagram of the initial configuration ($H_{\text{cruise}} = 18\,000$ m) [8]

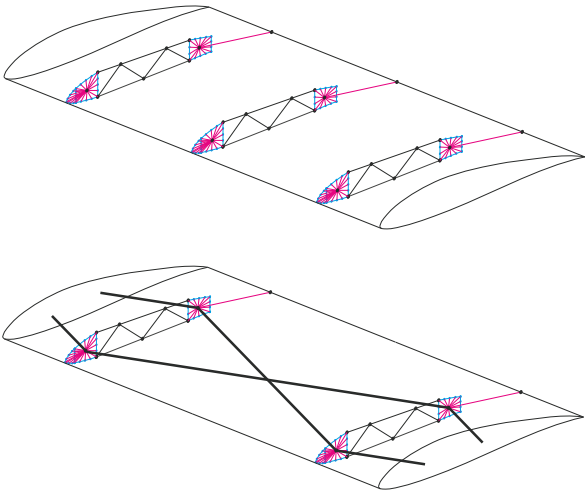

Fig. 30 Horizontal wing structures with internal braces [8]

Such a solution changes the structural modes of the SPB, making the natural frequencies of the system higher and removing any dynamic instability, as Table 5 and Fig. 31 show.

Finally, the previous analyses have been performed also at sea level conditions, for trim speed between 10 and 20 m/s, showing the absence of dynamic instability.

Table 5 Structural modes of the final configuration

Mode	Frequency [Hz]	Deformation
1	0.07	Bending out of the horizontal plane (mainly)
2	0.30	Torsion around wingspan direction (mainly)
3	0.31	Bending out of the horizontal plane (mainly)
4	0.40	Bending and torsion
5	0.72	Bending of vertical wings
6	0.76	Bending out of the horizontal plane (mainly)

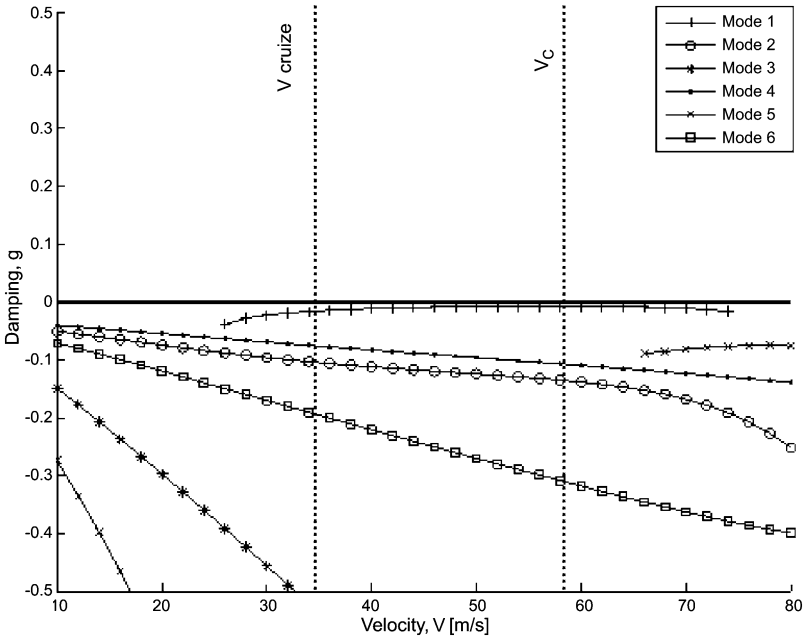

Fig. 31 Flutter diagram of the final configuration ($H_{\text{cruise}} = 18\,000$ m) [8]

7 Conclusions

The present paper has shown some of the outcomes of a research concerning the design of solar powered unmanned biplanes (SPB) for High Altitude Long Endurance (HALE) missions, whose architecture has been chosen in order to increase the structural stiffness without reducing the aerodynamic efficiency.

Inspired by several years of studies on box-wing airplanes at the Department of Aerospace Engineering (DIA) of Pisa, the main tasks of the present research have been the definition of a design methodology and the design of an SPB configuration able to fulfill the HALE flight requirements defined by DARPA within the *Vulture II*

program: to fly continuously in each year's day, at latitudes up to 45° and altitudes above 18 000 m.

The SPB layout has been presented, and, by means of some assumptions, a small set of geometric variables has been defined for the SPB description.

Two kinds of mission have been object of study: a first one for telecommunication (TLC), in which the aircraft has antennas as payload and operates on big areas (100–1000 km), and a second one for remote sensing purposes (IRS), in which the payload consists of electro-optical sensors and the operating area is much smaller ($<$10 km).

The design procedure, called "sizing process", has been described, presenting each model implemented in it. These are: the aerodynamic model, whose main task is to define the minimum required power conditions; the flight mechanic model, which is coupled with a Mass Balance model and aims to meet the stability and trim requirements; the energy balance section, in which the fulfillment of the endurance requirement is verified and the energy accumulation system is sized; the structural model, whose result is the structural components sizing, under a maximum stress constraint; and, finally, the propulsion system sizing, which defines the dimension of motors on the basis of the maximum power request.

For TLC missions, an SPB able to meet DARPA requirements has been found, and its characteristics have been shown, underlining that the predicted aerodynamic efficiency is comparable to those ones of flying wing and wing-tail configurations. A flexibility analysis has been carried out by means of a tool called Operating Domain, which has been applied in order to investigate the aircraft capabilities of performing both TLC and IRS missions under different altitude–latitude–day conditions. It has been found that it is possible to operate continuously at altitudes above 20 000 m for latitudes up to 16° in the case of TLC missions and 4° for IRS missions. On the other hand, given the minimum altitude of 16 000 m, the operating latitudes can reach 50° (TLC) and 38° (IRS).

In conclusion, the SPB configuration has been an object of a structural design review and an aeroelastic analysis, which have brought to some modifications: for horizontal wings, multi-box spars have been introduced to fulfill static and buckling loads requirements, internal braces have been added to avoid flutter phenomena, internal braces have been adopted also on vertical wings in order to minimize ground deformations, and, finally, the accumulators distribution along wingspan has been modified to reduce deformations and steady aeroelasticity effects on horizontal wings.

Acknowledgements My thanks go to all the people who worked with me on this topic at Department of Aerospace Engineering and, in particular, to the former students Paolo Rossi, Maurizio Borghi, Pasquale Cantisani, Luca Montanelli, Andrea Isoppo and Matteo Moisè. I also want to thank Prof. Aldo Frediani and Prof. Giuseppe Buttazzo for giving me the opportunity of presenting this work at the "Variational Analysis and Aerospace Engineering II" Workshop.

Appendix

This section contains information about the characteristics of main components taken into account for the design of SPBs (Table 6).

Table 6 Components data

Solar Cells	
Bi-facial Monocrystalline Silicon	
Efficiency (front)	20%
Efficiency (back)	17%
Density	0.32 kg/m^2
Solar Array	
Evaporated Back-Contacts [7, 13]	
Fill Factor	81%
Efficiency (@ 10% Albedo)	18%
Efficiency (@ 40% Albedo)	22%
Density	0.46 kg/m^2
Accumulators	
Li-S Rechargeable Batteries	
Energy Density (ε_g)	350 Wh/kg
Charge/Discharge Efficiency	99.7%
Life Cycles	100
Motors	
Brushless Direct Current Motors	
Efficiency	95%
Propellers	
Type	3-blade
Diameter	2 m
Efficiency	80%

References

1. Andress, K., Cebik, L.B., Severns, R., Lewallen, R., Witt, F.: The ARRL Antenna Book, 19th edn. (2000)
2. Borghi, M.: Progetto aerodinamico di un velivolo high altitude long endurance (HALE) ad energia solare. Master's thesis, University of Pisa, Department of Aerospace Engineering (2008) (Italian)
3. Cantisani, P.: Studi preliminari al progetto strutturale di un velivolo UAV biplano ad energia solare per missioni HALE (high altitude long endurance). Master's thesis, University of Pisa, Department of Aerospace Engineering (2008) (Italian)
4. Cipolla, V.: Design of solar powered high altitude long endurance unmanned biplanes. PhD thesis, University of Pisa, Ph.D. Course in Aerospace Engineering (2010)
5. DARPA: Vulture II, broad agency announcement. Technical Report DARPA-BAA-10-09, Defense Advanced Research Projects Agency (DARPA) (November 2009)
6. Duffie, J.A., Beckman, W.A.: Solar Engineering of Thermal Processes. Wiley, New York (1991)
7. Hubner, A., Aberle, A.G., Hezel, R.: Cost-effective bifacial silicon solar cells with 19% front and 18% rear efficiency. In: 14th European Photovoltaic Solar Energy Conference (1992)
8. Isoppo, A., Moisè, M.: Analisi aeroelastica mediante software MSC Nastran di un biplano UAV ad energia solare per missioni di tipo hale. Master's thesis, University of Pisa, Department of Aerospace Engineering (2011) (Italian)

9. Montanelli, L.: Analisi FEM di velivoli HALE-UAV ad energia solare e modelli di predizione del peso strutturale. Master's thesis, University of Pisa, Department of Aerospace Engineering (2010) (Italian)
10. Raymer, D.P.: Aircraft Design: A Conceptual Approach, 4th edn. AIAA Education Series. AIAA, Reston (2006)
11. Rizzo, E., Frediani, A.: A model for solar powered aircraft preliminary design. Aeronaut. J. **112**(1128), 57–78 (2008)
12. Rossi, P.: Studio di fattibilità di un sistema di conversione dell'energia solare per un velivolo a propulsione elettrica. Master's thesis, University of Pisa, Dipartimento di Ingegneria dell'Informazione (2007) (Italian)
13. Untila, G., Kost, T., Chebotareva, A., Zaks, M., Sitnikov, A., Solodukha, O.: A new type of high-efficiency bifacial silicon solar cell with external busbars and a current-collecting wire grid. Semiconductors **39**(11), 1346–1351 (2005)